Journal of Membrane Science 584 (2019) 79–88

Contents lists available at ScienceDirect

Journal of Membrane Science

journal homepage: www.elsevier.com/locate/memsci

Selective separation of CO_2 using novel mixed matrix membranes based on Pebax and liquid-like nanoparticle organic hybrid materials

Junfeng Wang[a], Wenjuan Fang[a], Jianquan Luo[a], Ming Gao[b], Yinhua Wan[a,**], Suojiang Zhang[b], Xiangping Zhang[b], Ah-Hyung Alissa Park[b,*]

[a] State Key Laboratory of Biochemical Engineering, Institute of Process Engineering, University of the Chinese Academy of Sciences, Chinese Academy of Sciences, Beijing, 100190, China

[b] Departments of Earth & Environmental Engineering and Chemical Engineering, Lenfest Center for Sustainable Energy, Columbia University, 500 W. 120th Street, New York, NY, 10027, USA

ARTICLE INFO

Keywords:
NOHM-I-HPE
Pebax1657
Mixed matrix membrane
CO_2 separation

ABSTRACT

Pebax1657 is known as a promising polymeric membrane material for CO_2 separation. In order to further improve its gas separation performance, different polymers containing ethylene oxide (EO) groups are incorporated into the Pebax1657 matrix to form mixed matrix membranes (MMMs). Liquid-like nanoparticle organic hybrid materials (NOHM-I-HPE, "I" stands for "ionic bond" and "HPE" refers to polyetheramine ("PE") with a high ("H") ether group content), which are made of polyetheramine chains tethered onto functionalized silica nanoparticles, have shown high solubility of CO_2. In this study, the homogenous NOHM-I-HPE/Pebax1657 MMMs with different NOHM-I-HPE loadings are prepared and investigated. The results indicate that the addition of NOHM-I-HPE leads to a decrease in glass transition temperature of Pebax1657 and an increase in EO content of the MMMs. Influences of NOHM-I-HPE content on CO_2, N_2 and CH_4 permeations are investigated at 23 °C and 1 bar. For the NOHM-I-HPE loading ranging from 0 to 60 wt%, solubility coefficients of the MMMs for CO_2 greatly increase from 1.16 to 3.84 cm^3 (STP)/(cm^3·bar), while those for CH_4 and N_2 only increase from 0.078 to 0.094 cm^3 (STP)/(cm^3·bar) and from 0.013 to 0.026 cm^3 (STP)/(cm^3·bar), respectively. Although the CO_2/N_2 selectivity slightly decreases with an increase in the NOHM-I-HPE loading, the CO_2/CH_4 selectivity is improved in the newly developed NOHM-I-HPE/Pebax1657 MMMs. These results indicate that the NOHM-I-HPE/Pebax1657 MMMs are very promising candidates for selective CO_2 separation for various energy related applications.

1. Introduction

CO_2 separation from large point sources has become a global and urgent issue since the escalating atmospheric concentration of CO_2 is threatening the delicate balance on Earth. Conventional technology for the separation of CO_2 is chemical absorption using amine-based solvents [1]. Although offering fast kinetics and high CO_2 capture capacities, amine scrubbing still faces a number of challenges including a high energy demand, the degradation of the amine, the release of volatile organic compounds and the risk of equipment corrosion. Therefore, some alternative technologies, such as anhydrous solvents [2,3], cryogenic distillation [4,5], membrane separation [6,7] and solid sorbents [8,9] have been proposed and developed for CO_2 separation. Among these technologies, membrane separation with a number of advantages, such as easy fabrication of flexible and compact devices, low energy requirements, low capital and operating costs, *etc.*, may be a promising approach for separating CO_2 from various gas mixtures.

Over the past several decades, the application of polymer-based gas separation membranes has drawn more attention because of their high permeability and selectivity [10,11]. For homopolymer membranes, such as polyamide (PA), polyimide (PI) and poly(dimethylsiloxane) (PDMS), their gas permeation properties mainly depend on the polymeric structure. A major drawback of homopolymer membrane is the trade-off limitation between permeability and selectivity, which is illustrated as the upper bound curve proposed by Robeson [12]. To deal with this trade-off, block copolymers based on poly(ethylene oxide) (PEO), such as poly(ether-*b*-amide) (Pebax), PEO-PI and PEO-PBT (poly (butylene terephthalate)) were synthesized by introducing PEO

* Corresponding author.
** Corresponding author.
E-mail addresses: yhwan@home.ipe.ac.cn (Y. Wan), ap2622@columbia.edu (A.-H.A. Park).

https://doi.org/10.1016/j.memsci.2019.04.079
Received 25 November 2018; Received in revised form 23 April 2019; Accepted 30 April 2019
Available online 07 May 2019
0376-7388/

segments into the polymer structure of homopolymer membrane [13–16]. Such block copolymers exhibits excellent CO_2 selectivity over other gases due to the strong dipole-quadrupole interactions between the polar ethylene oxide (EO) groups and CO_2 molecules, while their CO_2 permeability is not compromised [17–21]. Among these block copolymers, Pebax is a commercially available thermoplastic elastomer and a great candidate materials for CO_2 separation membrane.

In order to further improve the separation efficiency of the Pebax membrane, various methods, such as physical blending and chemical cross-linking, have been implemented to increase the total amorphous PEO content in the membrane. By incorporating poly(ethylene glycol) (PEG) into Pebax1657, Car and Reijerkerk et al. [22,23] prepared PEG/Pebax1657 blended membranes. The CO_2 permeability of PEG/Pebax1657 blended membrane with 50 wt% PEG loading was double that of Pebax1657, and the selectivity of CO_2/H_2 also increased due to high affinity between CO_2 and PEG. Reijerkerk et al. [24] also prepared the Pebax blended membrane containing poly(dimethyl siloxane) (PDMS) and PEG. The PDMS-PEG blended Pebax membrane with 50 wt % PDMS-PEG loading exhibited a CO_2 permeability of 532 Barrer, which was greater than that of the neat Pebax membrane (CO_2 permeability of 98 Barrer). The PEG diacrylate (PEGDA) was used to prepare fabricate PEGDA/Pebax1657 blended membranes by Ghadimi et al. [25] by adding PEGDA to Pebax1657 matrix. These membranes showed higher permeability for CO_2 than those for CH_4 and N_2, thereby the selectivity of CO_2 over the two gases was enhanced. Yave et al. [26] reported that the CO_2 permeability of the PEG dimethylether (PEGDME)/Pebax1657 blended membrane with 50 wt% PEGDME loading increased eight-fold.

Other polymeric materials have also been developed to capture CO_2. Nanoparticle organic hybrid material (NOHM-I-HPE, "I" stands for "Ionic bond" and "HPE" refers to polyetheramine ("PE") with a high ("H") ether group content), which consists of inorganic nanosized silica and ionically tethered organic canopy species (i.e., polyetheramine) were found to exhibit a good selectivity for CO_2 against N_2 [27–30]. NOHM-I-HPE offers an organic-inorganic hybrid matrix, which can tune both affinity and accessibility to CO_2. Compared to the amine-based reagents, the separation of CO_2 through physical interactions or weak Lewis acid-base interactions is particularly attractive because the stripping of CO_2 can be operated under much milder conditions [27]. Especially, NOHM-I-HPE possesses a high content of flexible amorphous PEO segments and 0.4 mol of CO_2 can be captured by 1 kg of solvent at 3.2 MPa [27], suggesting that the incorporation of NOHM-I-HPE into the Pebax matrix could enhance CO_2 separation performance of the membrane.

In this study, NOHM-I-HPE/Pebax1657 mixed matrix membranes (MMMs) with different NOHM-I-HPE loadings were prepared. The objective of this work is to investigate the effect of NOHM-I-HPE loading on the gas transport properties of the NOHM-I-HPE/Pebax1657 MMMs, and gain insight into the thermal properties, morphology, structure as well as mechanical properties of these MMMs. Firstly, the prepared MMMs and their corresponding precursors were characterized by thermogravimetric analysis (TGA), differential scanning calorimetry (DSC), fourier transform infrared (FT-IR), scanning electron microscope (SEM), and tensile tests. Then, the permeabilities of NOHM-I-HPE/Pebax1657 MMMs for pure gases (i.e., CO_2, CH_4 and N_2) and gas mixtures (CO_2/N_2 and CO_2/CH_4) were measured at 23 °C and 1 bar. Finally, the performance of the membrane to separate CO_2 over CH_4 and N_2 were evaluated in a mixed gas steam.

2. Experimental section

2.1. Materials

LUDOX SM-30 silica (7 nm in diameter) and ion exchange resin (DowexTM HCR-W2) were supplied by Sigma-Aldirch (Milwaukee, WI) and Dow Chemical Co. (Midland, MI), respectively. 3-(trihydroxysilyl)-1-propane sulfonic acid (silane) and Jeffamine M-2070 (HPE, 1600–2200 g/mol for PEO) were purchased from Gelest Inc. (Morrisville, PA) and Huntsman Co. (The Woodlands, TX), respectively. Pebax1657 which is composed of a polyamide block and a polyether block (PE), was purchased from Arkema Inc (Paris, France). Ethanol was supplied by Beijing Chemical Reagent Co. (Beijing, China). It was reagent grade and used directly without further purification. CO_2 (99.99%), N_2 (99.99%) and CH_4 (99.99%) were supplied by Hai-Pu Gas Industry Co. (Beijing, China).

2.2. Synthesis of NOHM-I-HPE

NOHM-I-HPE was synthesized using the previously reported method [27]. Firstly, LUDOX SM-30 silica and 3-(trihydroxysilyl)-1-propane sulfonic acid were firstly diluted with deionized (DI) water to prepare 3 wt% silica suspension and 6 wt% silane solution, respectively. The silica suspension was added to the silane solution, and then the mixture was adjusted to pH 5 by adding 1 M sodium hydroxide. Next, the mixture was incubated at 343 K for 12 h with vigorous stirring. To remove excess silane, the functionalized silica suspension was dialyzed against deionized water for 48 h. The ion exchange resin was employed to remove sodium ions from the dialyzed solution and to protonate the sulfonate group present on the surface of the nanoparticles. Finally, HPE was diluted to 10 wt% solution and added dropwise to the functionalized nanoparticle suspension. After the excess water was removed under reduced pressure at 308 K for 36 h, the liquid NOHM-I-HPE was obtained.

2.3. Membrane fabrication

NOHM-I-HPE was incorporated in Pebax1657 via the solution casting method. To prepare a solution for the flat-sheet membrane, a mixture of ethanol/water (70/30 wt%) was used as a solvent. Firstly, a Pebax solution was prepared by dissolving Pebax1657 in the solvent at 80 °C under reflux and vigorously stirred for 4 h to obtain a homogenous polymeric solution. After the solution was cooled down to room temperature, a given amount of NOHM-I-HPE, defined by Eq. (1), was completely dispersed in 10 mL solvent, and then mixed with the Pebax solution followed by stirring for another 4 h. The resulting mixture was sonicated for 30 min to degas and then poured into a flat-bottom Teflon mold. Subsequently, the solvent was evaporated at 40 °C for 24 h. After being carefully peeled off from the Teflon mold, the nascent membranes were further dried for 3 days at 40 °C under vacuum to eliminate any residual solvent. Finally, the average thickness of the resultant dense NOHM-I-HPE/Pebax1657 MMMs was measured using a digital screw micrometer (IP65, Mitutoyo) and it was in the range of 80–100 μm. In addition, a pure Pebax1657 membrane was also prepared in the similar procedure as a base case.

$$\text{NOHM} - \text{I} - \text{HPE loading (wt.\%)} = \left(\frac{m_{\text{NOHM-I-HPE}}}{m_{\text{NOHM-I-HPE}} + m_{\text{Pebax}}}\right) \times 100\% \quad (1)$$

In this study, NOHM-I-HPE loadings ranging from 0 to 60 wt% were investigated since the mixed matrix membrane with NOHM-I-HPE loading of more than 60 wt% could not be synthesized due to its low elasticity. The chemical structures of pure Pebax1657 and NOHM-I-HPE are shown in Supporting Information Fig. S1.

2.4. Membrane characterization

2.4.1. Fourier transform infrared (FT-IR)

A Nicolet iS50 spectrometer (Thermo Fisher Scientific Corporation, USA) was used to verify the chemical compositions of the membrane surface. FT-IR spectra were acquired. The scanning frequency range was 4000-500 cm^{-1} under ambient conditions, with spectral resolution

of 2 cm^{-1}.

2.4.2. X-ray photoelectron spectroscopy (XPS)

XPS analysis was performed using a Thermo escalab 250Xi (Thermo Nicolet Instrument Corporation, WI, USA) equipped with a monochromatic Al Ka radiation (1486.6 eV) at an operating power of 150 W. The binding energy data were calibrated in term of the C 1s signal of ambient hydrocarbons (C–H and C–C) at 284.8 eV. Surface survey data were collected followed by high resolution scans over C 1s (279–299 eV), O 1s (525–545 eV), N 1s (392–414 eV) and Si 1s (95–114 eV). Peak areas were calculated using the Gaussian fit program.

2.4.3. Scanning electron microscope (SEM)

A SEM (JSM-7001F, Japan) was employed to characterize the prepared membranes. The surface and cross-section morphologies of Pebax-based membranes were analyzed at a voltage of 5 kV and a current of 10 mA. Prior to the surface analysis, the membrane sample was sputtered with a thin layer of gold using an Emitech sputtering device (JSM-6500, Japan). For the cross-section analysis, the membrane sample was cryogenically fractured in liquid nitrogen and sputtered, and then the cross-section morphology was taken.

2.4.4. Differential scanning calorimetry (DSC)

A Mettler-Toledo DSC 822e instrument (TA Instruments, USA) was used to study the effect of NOHM-I-HPE loading upon the thermal transitions of the prepared Pebax-based membranes. For each membrane, more than three samples were collected and measured to ensure the reproducibility of the experimental results. For each sample, temperatures at glass transition (T_g) and melting point (T_m) were determined using 3 cooling processes and 2 heating processes. A small amount of sample was first weighted and hermetically sealed into an aluminum pan. The testing sample was cooled down from room temperature to −100 °C, and then heated from −100 °C to 250 °C at a rate of 10 °C/min in the first DSC cycle. The cooling and heating steps were repeated twice. At last, the temperature was lowered to room temperature to complete the measurement. Through analyzing the second heating process, T_g and T_m were determined. In addition, the degree of crystallinity in hard segments of the membrane (X_{PA}) was calculated using Eq. (2) based on the DSC data.

$$X_{PA} = \frac{\Delta H_m}{(1 - 60\%)\phi\Delta H_m^0} \times 100 \tag{2}$$

where ΔH_m is the melting enthalpy determined by integrating the area under the melting peak in the DSC curves, φ is the weight percentage of the soft or hard phase in the blended membrane, ΔH_m^0 is the enthalpy of the pure crystalline phase. ΔH_m^0 of hard segments is 230 J/g taken from literature [14]. The reproducibilities in measuring T_g and T_m were used to assess the relative error for this technique and they were found to be less than 0.2 °C.

2.4.5. Thermogravimetric analysis (TGA)

The thermal stabilities of pure components and NOHM-I-HPE/Pebax1657 MMMs were evaluated using a TGA Q50 (TA Instruments, USA). Each time, about 8 mg of sample was accurately weighted before the calcination process. The samples were heated from room temperature to 800 °C with a temperature ramping rate of 10 K/min under high-purity nitrogen flow (flow rate: 40 mL/min) in the in-built platinum pan of the TGA instrument.

2.4.6. Mechanical properties

The tensile stress-strain characteristics of membranes were studied using an Instron 3365 mechanical testing machine (Instron Corp., USA) fitted with a 100 N load cell. The tensile experiments were performed at room temperature (25 °C, 50% relative humidity) with a crosshead speed of 20 mm/min. The testing speed was set at a rate of 20 mm/min. All samples were prepared with a width of 10 mm and a length of 50 mm. The reported values of all the mechanical properties were averaged over five independent measurements. The reproducibility in measuring mechanical property was used to assess the relative error for this technique, and it was less than 2%.

3. Permeability of gases

All measurements were performed at a constant temperature of 23 °C and a feed pressure of 1 bar. Before analysis, the membrane samples were carefully evacuated to remove previously dissolved species. A total membrane area of 4.9 cm^2 was used. For each membrane, three membrane samples were tested to ensure the reproducibility of the experiment results. Physical properties of gases were listed in Supporting Information Table S1 [31].

The transport mechanism of gases through a non-porous, dense and polymeric membrane is usually assumed to follow a solution-diffusion process [32–34]. The permeability of pure gases was determined with the constant volume/variable pressure ("time lag") method using vacuum in the downstream [35,36]. Compared to flux, permeability (P_i), which is a material property, is less dependent on the membrane thickness and the *trans*-membrane pressure difference. Permeability and diffusion coefficient (D_i) of gas i can be determined from the pressure increase curves obtained during the "time-lag" experiments using the following equations [35]:

$$P_i = \frac{V_i}{A} \times \frac{273.15}{T} \times \frac{l}{p_s(p_f - p_p)} \times \frac{dp}{dt} \tag{3}$$

$$D_i = \frac{l^2}{6\theta} \tag{4}$$

where V_i, l, A, T and p_s are permeated volume of gas i (cm^3), membrane thickness (cm), membrane area (cm^2), operating temperature (K) and standard pressure (1 bar), respectively. p_f and p_p are upstream and downstream pressures (cmHg), $\frac{dp}{dt}$ is the pressure increment with time in the downstream chamber (bar·s^{-1}), and θ is the lag time (s). The ideal gas permeability through a membrane can also be described as the product of solubility coefficient (S_i) and diffusion coefficient of gas i.

$$P_i = S_i \times D_i \tag{5}$$

Therefore, S_i which generally depends on the gas molecule condensability, the interactions between gas and membrane material as well as morphological features of the membrane material, can be obtained based on the permeability and diffusion coefficient (Eq. (5)). Also, the selectivity (α_{ij}), which is often treated as a material property like permeability, can be calculated by taking the ratio of the ideal gas permeability for a given gas pair (i and j):

$$\alpha_{ij} = \frac{P_i}{P_j} = \frac{S_i D_i}{S_j D_j} \tag{6}$$

To further testify the membrane separation performances for mixed gases, i.e. CO_2/N_2 (15/85 vol.%) and CO_2/CH_4 (30/70 vol.%), permeation performances of the membranes were determined with the constant pressure/variable volume method at 23 °C and 1 bar [36]. The concentration of each gas in the feed and permeate gases was measured by an Agilent 6980 N gas chromatography (Agilent Corp., USA) equipped with a thermal conductive detector. And then permeability of gas i as well as selectivity of gas i to gas j can be calculated using Eq. (3) and Eq. (6), respectively. The reproducibility in measuring permeability was used to assess the relative error for this technique, and it was less than 4.5%.

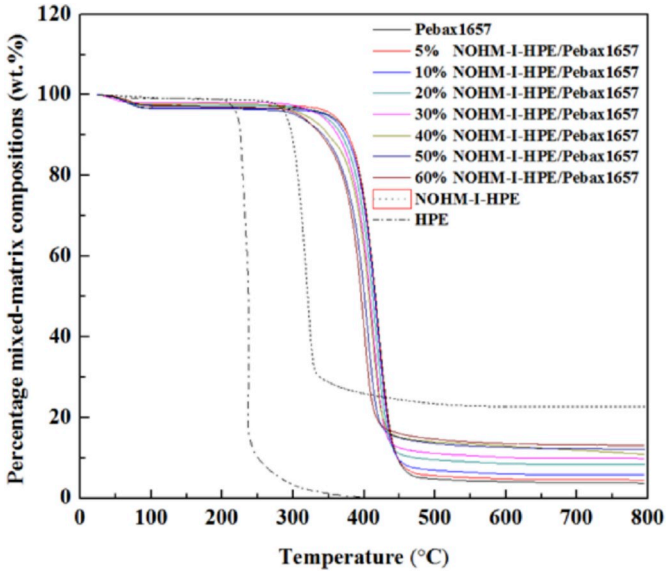

Fig. 1. Thermal stabilities of pure components and NOHM-I-HPE/Pebax1657 MMMs as a function of temperature.

4. Results and discussion

4.1. Enhanced thermal properties of membranes

Thermogravimetric studies were conducted to assess thermal stabilities of pure components and NOHM-I-HPE/Pebax1657 MMMs with different NOHM-I-HPE loadings. Fig. 1 shows TGA curves of all the samples as a function of temperature. The improved thermal stability of NOHM-I-HPE leading to its negligible vapor pressure has already been reported, which is one of the factors making NOHMs great alternatives of aqueous CO_2 capture solvents [37]. Compared to neat Pebax1657, NOHM-I-HPE was not as thermally stable, but interestingly the NOHM-I-HPE/Pebax1657 MMMs exhibited thermal stabilities closer to that of Pebax1657 than NOHM-I-HPE. Such an enhancement might be resulted from a strong intermolecular interaction between NOHM-I-HPE and Pebax1657. The decomposition temperature of Pebax1657 was about 362 °C, which was close to that reported by Dai et al. [38]. With an increase in NOHM-I-HPE loading, the thermal stability of the MMM decreased slightly but it was clear that NOHM-I-HPE within the membrane was further stabilized and would be able to participate in CO_2 capture at even higher temperatures than previously studied.

The thermal properties of NOHM-I-HPE, pure Pebax1657 and NOHM-I-HPE/Pebax1657 MMMs were also investigated via DSC analysis. The results are listed in Supporting Information Table S2. It was found that for each membrane only two melting temperatures were observed, mainly resulting from a microphase-separated structure in block copolymers [39]. For pure Pebax1657 membrane, the lower T_m was attributed to the melting of PEO crystals, whereas the higher T_m corresponded to melting of PA crystalline phases [22,40]. With the addition of NOHM-I-HPE, a slight decrease in melting temperatures of soft PE segments in Pebax1657 and a non-discernible change in those of hard PA segments were observed. As the content of NOHM-I-HPE was increased to 60 wt%, the melting temperature of soft segments in the MMM was 12.3 °C, which was a slightly lower than that in pure Pebax1657 (13.8 °C). Such a decrease in T_m of the PEO crystalline phase in the MMMs with increased NOHM-I-HPE loading was probably due to the presence of NOHM-I-HPE induced deterioration of the Pebax1657 crystal structure. The crystallinity of PA in prepared membranes was calculated using Eq. (2) and the enthalpy of fusion obtained from the area of the melting peak in the second DSC cycle. X_{PA} of the pure Pebax1657 membrane was 25.04%, which was consistent with that reported by Rabiee et al. [41]. With the increased NOHM-I-HPE loading in the MMMs, the enthalpy of fusion and the crystallinity of PA decreased. As shown in Supporting Information Table S2, the enthalpy of fusion of PA for the NOHM-I-HPE/Pebax1657 MMM with 60 wt% NOHM-I-HPE loading was only 7.07 J/g, which was less than one third of the neat Pebax membrane (23.04 J/g).

T_g of PEO block in pure Pebax1657 was found to be −52.6 °C, which was nearly the same as that (−52 °C) reported by Rahman et al. [42]. T_g of NOHM-I-HPE (−68.0 °C) was lower than that of pure Pebax1657 indicating that the mobility of polyether segments in NOHM-I-HPE was higher than that in Pebax1657 because T_g was a crude indicator of the mobility of polymer segments. For each NOHM-I-HPE/Pebax1657 MMM, only one T_g was observed, indicating the good miscibility between NOHM-I-HPE and Pebax1657. T_g decreased with an increase in NOHM-I-HPE loading, and when the NOHM-I-HPE loading in the MMM was up to 60 wt%, T_g reduced to −60.1 °C, which was close to that of pure NOHM-I-HPE. This suggested that the addition of NOHM-I-HPE caused an increase in chain mobility in the MMM, and thus, the transition to a rubbery state could occur at a lower temperature. Also, the changes in T_g can be related with the altered fractional free volume (FFV) of the polymer [43]. Therefore, such a decrease in T_g led to the hypothesis that NOHM-I-HPE acted as an amorphous phase and probably led to higher FFV in the blended membrane matrix. This phenomenon could alter the gas diffusion performance of the MMM (this will be illustrated in the next section). Rahman et al. [42] also found that the incorporation of polyoctahedral oligomeric silsesquioxanes (POSS) functionalized with PEG in Pebax1657 resulted in a decreased T_g and crystallinity of the nanocomposite membranes.

4.2. Identification of chemical functional groups designed for gas separation

Chemical structures of NOHM-I-HPE/Pebax1657 MMMs along with their precursor materials were studied using FT-IR analysis shown in Fig. 2. The characteristic absorption bands of precursor materials (i.e., HPE, silane and silica) were clearly identified in the spectra of the NOHM-I-HPE. For HPE, broad bands around 1050 and 2850 cm^{-1} corresponded to C–O and CH_2 stretching vibrations, respectively. The protonated amine absorption bands between HPE and silane were found at 1530 cm^{-1} ($\delta_s(NH_3^+)$) and at 1630 cm^{-1} ($\delta_a(NH_3^+)$), indicating the formation of ionic bonding as suggested in Supporting Information Fig. S1 (top). For silane, the main characteristic absorption bands of Si–*O*–C stretching and SO_3^- stretching were observed in the region of 800–1250 cm^{-1}, which was broad overlapping. The characteristic absorption band near 1105 cm^{-1} was identified as Si–*O*–Si stretching vibration belonging to silica. All of these were consistent with those identified by Petit et al. [28]. The characteristic absorption bands of Pebax1657 were around 1640 and 3292 cm^{-1} and they were associated with H–N–C=O and -N-H groups, respectively. Saturated esters (O–C=O) as well as C–O in PE blocks showed characteristic absorption bands near 1733 and 1099 cm^{-1}, respectively [25,44].

As shown in Fig. 2, the main features of NOHM-I-HPE were clearly observed in the spectra of NOHM-I-HPE/Pebax1657 MMMs indicating that NOHM-I-HPE was present in the membranes and its chemistry was preserved. It should also be noted that the characteristic absorption band of C–O slightly shifted to a lower wavenumber (from 1099 cm^{-1} for Pebax1657 to around 1075 cm^{-1} for NOHM-I-HPE/Pebax). Moreover, with an increase in the NOHM-I-HPE loading in the MMMs, C–O peak became stronger due to a large amount of ether groups in NOHM-I-HPE.

In order to further investigate chemical functional groups existing in the membrane, XPS survey spectra of the pure Pebax1657 membrane and the NOHM-I-HPE/Pebax1657 MMM with 50 wt% NOHM-I-HPE loading were obtained. No Si signal was detected in the neat Pebax1657 membrane (Fig. 3(a)), whereas four characteristic XPS signals corresponding to C, O, N and Si were clearly observed in the MMM containing NOHM-I-HPE (Fig. 3(b)). In addition, with an increase in the

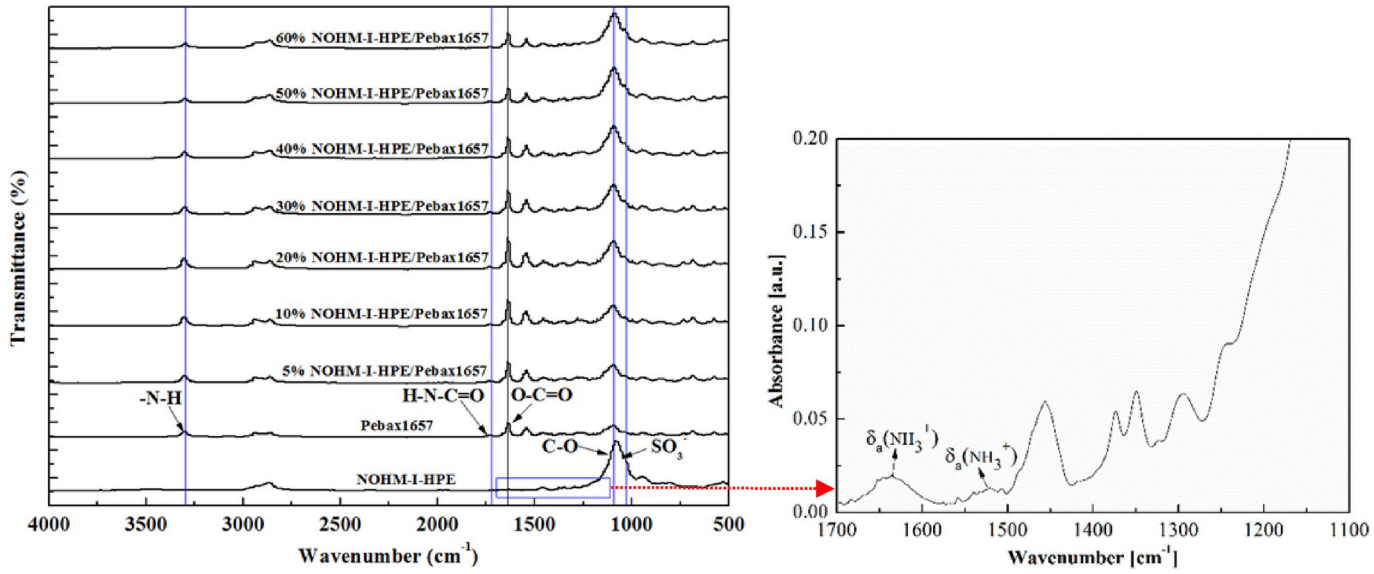

Fig. 2. FT-IR spectra of pure components and NOHM-I-HPE/Pebax1657 MMMs.

NOHM-I-HPE loading, the Si signal increased while those of C and N decreased slightly. The result indicated that NOHM-I-HPE was successfully incorporated in the NOHM-I-HPE/Pebax1657 MMMs. It is worth mentioning that the content of O in the MMM with 50 wt% NOHM-I-HPE loading increased by 14.37% compared to that of the pure Pebax1657 membrane. This illustrated that the content of ether oxygen groups in NOHM-I-HPE was higher than that in pure Pebax1657.

4.3. Morphological structures of membranes with different NOHM-I-HPE loadings

NOHM-I-HPE dispersed in the Pebax solution with ethanol/water binary solvent was used to produce the membrane. In order to verify the uniformity of the material dispersion and the absence of precipitation within the membrane, a series of SEM images were taken.

As shown in Fig. 4(a)-4(h), there were no defects or agglomerates, further indicating the great compactability and higher degree of interpentration between NOHM-I-HPE and Pebax1657. The surface of the membrane made of pure Pebax1657 revealed a needlelike structure, which corresponded to the PA hard segments of the polymer (Fig. 4(a)). The regions in between these needles corresponded to the PE soft segments. As shown in Fig. 4(b)–(h), the surface morphologies of the membranes changed as NOHM-I-HPE was incorporated into the matrix. With an increase in NOHM-I-HPE loading, the area of needlelike structures on the MMM surface decreased due to an reduction in the amount of PA segments, which was confirmed from the DSC result discussed earlier. Also, an increase in NOHM-I-HPE loading led to a change in the membrane surface roughness. The membranes with the NOHM-I-HPE loading from 0 to 30 wt%, the membrane surface were more uniform and smoother as the NOHM-I-HPE loading increased. This phenomenon was mainly due to the inter-pentration between NOHM-I-HPE and Pebax1657, which was also verified from a higher decomposition temperature of the NOHM-I-HPE/Pebax1657 MMM discussed earlier. But as the NOHM-I-HPE loading was increased beyond 30 wt%, the surface roughness of the NOHM-I-HPE/Pebax1657 MMM was visibly increased as shown in Fig. 4(f)-(h). This was because increased amount of NOHM-I-HPE containing nanosized particles were exposed to the surface of the membrane at higher NOHM-I-HPE loadings. The cross-sectional morphologies of three distinct samples (i.e., pure Pebax1657, and 20 and 50 wt% NOHM-I-HPE loadings) were also investigated and as shown in Fig. 5, a homogeneous morphology for all samples was observed regardless the surface roughness shown in Fig. 4. The average thickness of the membranes was measured to be around 80–100 μm.

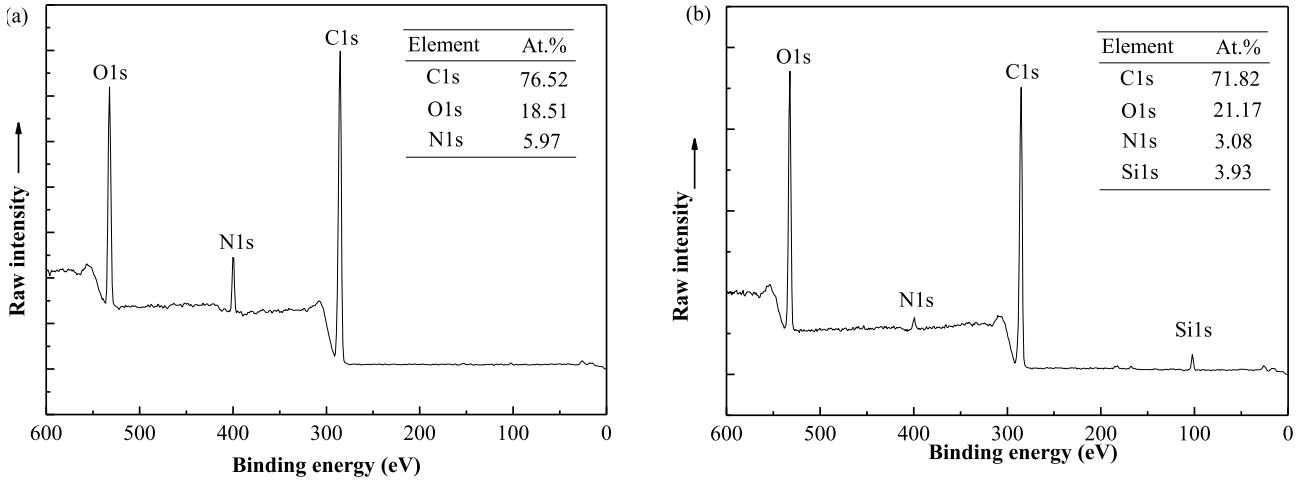

Fig. 3. XPS spectra of (a) Pebax1657 and (b) NOHM-I-HPE/Pebax1657 MMM with 50 wt% NOHM-I-HPE loading.

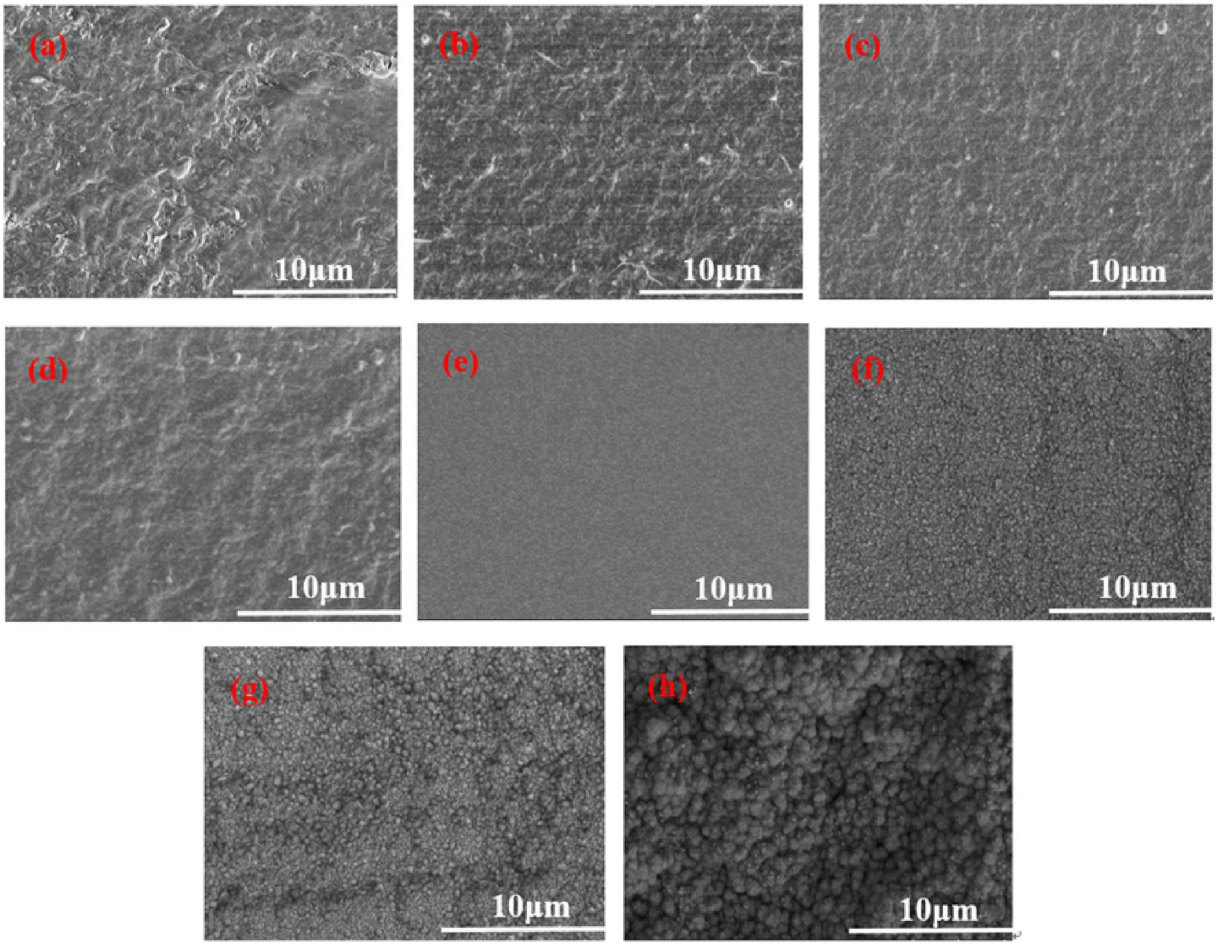

Fig. 4. Surface morphological structure of membranes based on (a) neat Pebax1657 and mixed matrix of NOHM-I-HPE/Pebax1657 at (b) 5 wt%, (c) 10 wt%, (d) 20 wt%, (e) 30 wt%, (f) 40 wt%, (g) 50 wt% and (h) 60 wt% NOHM-I-HPE loadings.

4.4. Effect of NOHM-I-HPE loading on mechanical properties of membranes

One of the important membrane properties is mechanical strength. Thus, tensile tests were performed to examine the mechanical property changes in the NOHM-I-HPE/Pebax1657 MMMs compared to pure Pebax1657. Tensile strength, Young's modulus and elongation at break of each sample are summarized in Supporting Information Table S3. Young´s modulus for the pure Pebax1657 membrane was 154.47 MPa, which was the same as the value (154.5 MPa) reported by Rabiee et al. [41]. An increment in the NOHM-I-HPE loading resulted in a decrease in tensile strength, Young's modulus and elongation at break of the MMMs. For the MMM with 60 wt% NOHM-I-HPE loading, the tensile strength, elongation at break and Young's modulus were only 2.10 MPa, 61.07% and 17.74 MPa, respectively. The addition of NOHM-I-HPE caused the decrease of relative amounts of hard PA and soft PE segments in the MMM, which were mainly responsible for the mechanical strength and elongation at break, respectively. In addition, part of the hard PA blocks in the Pebax1657 matrix may have been softened by NOHM-I-HPE acting as the amorphous phase. Therefore, the tensile strength of the mixed matrix membranes was lowered. This finding was consistent with the DSC results, which showed a reduction in crystallinity in hard segments (Supporting Information Table S2).

4.5. Gas transport behaviors through MMMs

The most important operational parameters of the membrane system are permeability and selectivity. A series of experiments were performed to investigate the gas transport behaviors through the prepared MMMs. First, pure gas permeabilities were measured through the neat Pebax1657 and the NOHM-I-HPE/Pebax1657 MMMs with

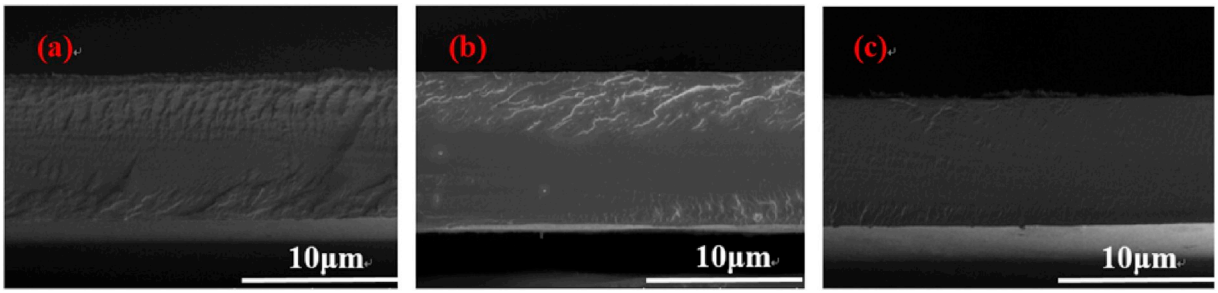

Fig. 5. Cross-sectional morphologies of (a) neat Pebax1657 membrane and NOHM-I-HPE/Pebax1657 MMMs with (b) 20 wt% and (c) 50 wt% NOHM-I-HPE loadings.

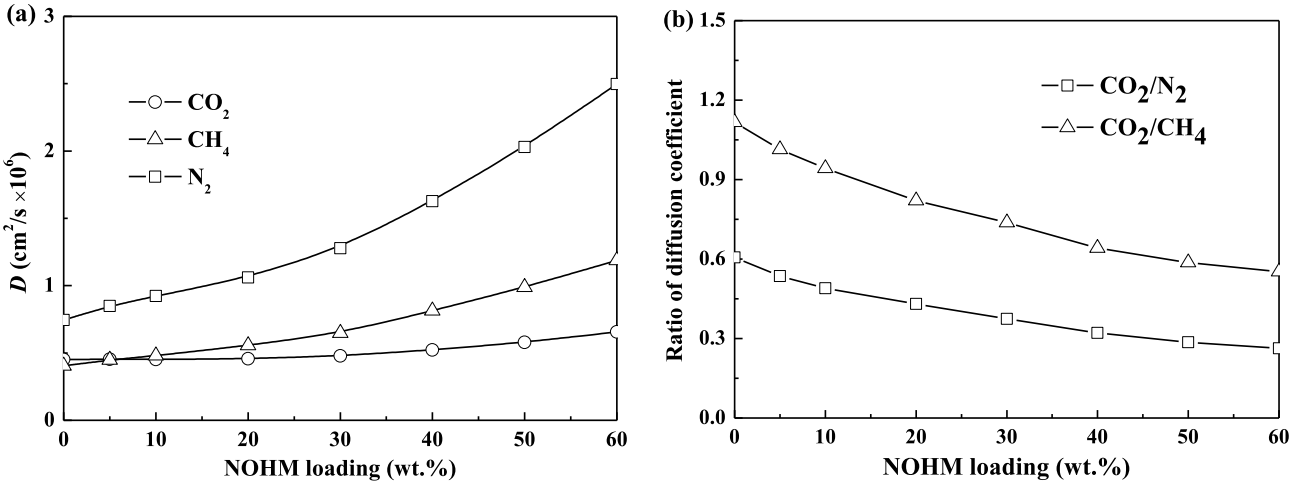

Fig. 6. Effect of NOHM-I-HPE loading on (a) diffusion coefficients (-○-, CO_2; -Δ-, CH_4; -□-, N_2) and (b) ratios of diffusion coefficients (-□-, CO_2/N_2; -Δ-, CO_2/CH_4) of neat Pebax1657 membrane and NOHM-I-HPE/Pebax1657 MMMs at 1 bar and 23 °C.

different NOHM-I-HPE loadings. Diffusion coefficients of three gases (i.e., CO_2, N_2 and CH_4) were obtained for different NOHM-I-HPE loading cases. As shown in Fig. 6(a), the diffusion coefficient of CO_2 was increased as a function of NOHM-I-HPE loading, although the difference was not very significant. When the NOHM-I-HPE loading was 60 wt%, the diffusion coefficient of CO_2 reached 0.66×10^{-6} cm^2/s. On the other hand, there were large increases in diffusion coefficients of CH_4 and N_2 with higher NOHM-I-HPE loadings in the prepared membranes, particularly greater than 30 wt%. Diffusion coefficients of N_2 and CH_4 were 2.50×10^{-6} and 1.19×10^{-6} cm^2/s, respectively, for the MMM at 60 wt% NOHM-I-HPE loading. The increment in diffusion coefficients for gases at higher NOHM-I-HPE loadings can be attributed to the following three factors: (1) the addition of NOHM-I-HPE resulted in more amorphous and flexible structure of the MMMs, which has been verified by various membrane characteristic tests (i.e., DSC, SEM and tensile analysis), (2) the decreasing crystallinity of the MMMs (as shown in Supporting Information Table S2) with an increase in NOHM-I-HPE loading may have resulted in an increase in FFV, and (3) NOHM-I-HPE containing flexible Si–*O*–Si linkages enhanced gas diffusivity, which would have been derived from the low energy barrier of rotation of the polymeric chains tethered to nanoparticles (as shown in Supporting Information Fig. S1) and the creation of favorable pathway for gas diffusion [29].

It can also be seen from Fig. 6(a) that diffusion coefficients of three gases in NOHM-I-HPE/Pebax1657 MMMs followed the order of $D(N_2) > D(CH_4) > D(CO_2)$, and this trend was most visible for the NOHM-I-HPE loading range of 20–60 wt%. N_2 diffused faster than CH_4 molecule, which was coincident with the kinetic diameters of the gases (Supporting Information Table S1). While CO_2 has the smallest kinetic diameter among three gases, its diffusivity was lowest because of the Lewis acid-base interaction between CO_2 and ether groups in NOHM-I-HPE reported in literature [27]. This chemical interaction of CO_2 with the mixed matrix membrane resulted in interesting relative diffusivity behaviors shown in Fig. 6(b). Ratios of diffusion coefficients of CO_2/N_2 and CO_2/CH_4 for the MMMs decreased with increasing NOHM-I-HPE loading because the rates of diffusion coefficient increase for N_2 and CH_4 were far higher than that for CO_2.

Next, solubility coefficients of the three gases were obtained using the permeability and diffusion coefficient (Eq. (5)). As shown in Fig. 7(a), the solubility of CO_2 in the MMM changed greatly as a function of NOHM-I-HPE loading (slope of 0.0453), whereas negligible changes were observed for the solubility of N_2 and CH_4 (slopes of 0.00022 and 0.00025, respectively). Solubility coefficient for CO_2 increased from 1.16 to 3.84 cm^3 (STP)/(cm^3·bar), while the values for CH_4 and N_2 minimally increased from 0.078 to 0.094 cm^3 (STP)/(cm^3·bar) and from 0.013 to 0.026 cm^3 (STP)/(cm^3·bar), respectively, as NOHM-I-HPE loading increased from 0 to 60 wt%. Even for the pure Pebax1657 membrane, CO_2 gas showed a high solubility in ethylene oxide units mainly due to the affinity of ether oxygen and CO_2. As discussed earlier, Park et al. have found that the ether-based material possessed the highest solubility for CO_2 owing to the dipole and quadrupole interaction between polar ether oxygen and CO_2, whereas N_2 was found to be almost insoluble in NOHM-I-HPE [27]. The addition of NOHM-I-HPE into Pebax1657 resulted in a higher content of ether oxygen units (as shown in Fig. 3) and lower content of non-sorbing crystals in the MMMs (as listed in Supporting Information Table S2). In turn, the larger quadrupole moment, higher polarizability as well as higher condensability of CO_2 in the membrane (as shown in Supporting Information Table S1) led to an increase in solubility of CO_2. For the NOHM-I-HPE/Pebax1657 MMM with the same NOHM-I-HPE loading, the order of solubility coefficient for the three gases was $S(CO_2) \gg > S(N_2) > S(CH_4)$. Note that the scale for CO_2 and N_2/CH_4 are orders of magnitude different. Fig. 7(b) shows the solubility ratios of CO_2/N_2 and CO_2/CH_4 for each MMM, which were far greater than one and they continued to increase as the NOHM-I-HPE loading increased. The increased CO_2 solubility and remarkably high solubility ratios towards CO_2 compared to N_2 and CH_4 illustrated a good potential of CO_2 separation from N_2 and CH_4 using the NOHM-I-HPE/Pebax1657 MMMs.

4.6. Gas separation selectivity of membranes and its comparision to the Robeson's upper bound

In order to investigate the overall performance of the NOHM-I-HPE/Pebax1657 MMMs, the relative permeability of gases should be discussed along with their diffusivity and solubility behaviors. Further analysis on the pure gas permeability and the ideal selectivity of CO_2 over N_2 and CH_4 of neat Pebax1657 and NOHM-I-HPE/Pebax1657 MMMs provided value insights into the potential of the developed MMM as a system to separate CO_2 from N_2 and CH_4. As shown in Fig. 8(a), compared to the neat Pebax1657 membrane, NOHM-I-HPE loaded membranes led to large increases in permeability of all the gases. Particularly, the permeability of CO_2 increased from 70.02 to 335.93 Barrer, while the values for CH_4 and N_2 increased from 4.20 to 14.91 Barrer and from 1.31 to 8.69 Barrer, respectively, as NOHM-I-HPE loading increased from 0 wt% to 60 wt%. Permeability of CO_2 for the MMM containing 60 wt% NOHM-I-HPE was nearly five times higher than that of the neat Pebax1657 membrane. The permeabilities of three gases followed the order of $P(CO_2) \gg > P(CH_4) > P(N_2)$. This can be explained by solution-diffusion mechanism [45]. For the NOHM-I-HPE/Pebax1657 MMMs, gas permeabilities were controlled by both gas

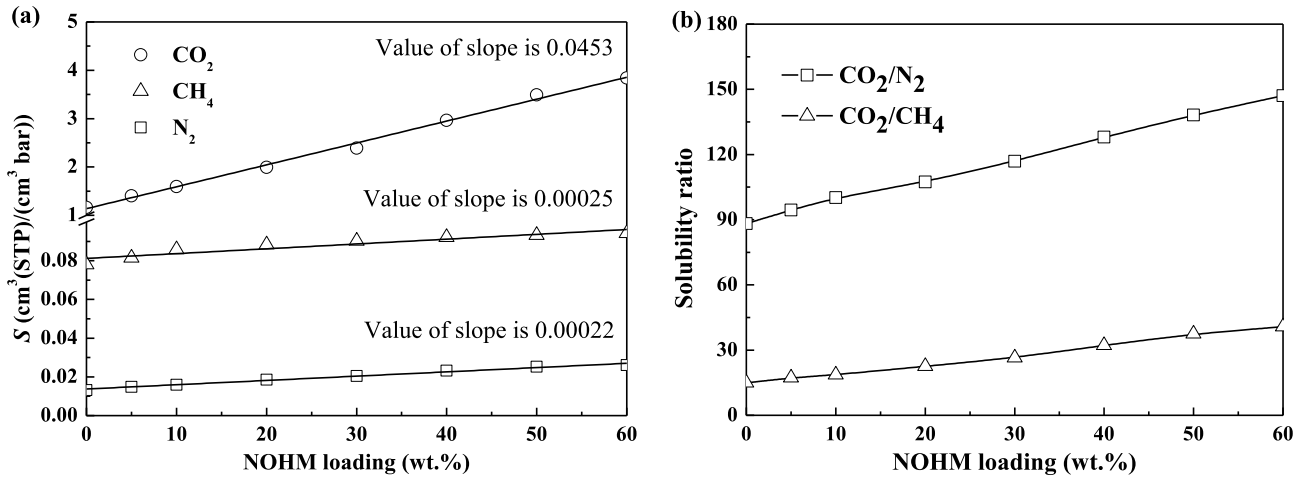

Fig. 7. Effect of NOHM-I-HPE loading on (a) solubility coefficients (○, CO_2; Δ, CH_4; □, N_2; — Correlated results) and (b) solubility ratios (-□-, CO_2/N_2; -Δ-, CO_2/CH_4) of neat Pebax1657 membrane and NOHM-I-HPE/Pebax1657 MMMs at 1 bar and 23 °C.

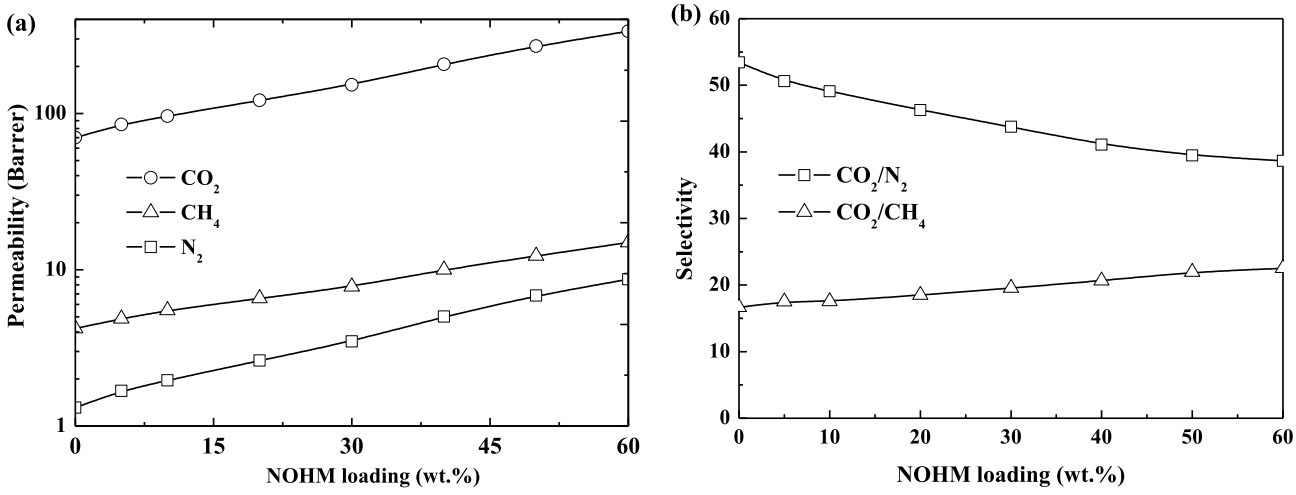

Fig. 8. Effect of NOHM-I-HPE loading on (a) permeabilities (-○-, CO_2; -Δ-, CH_4; -□-, N_2) and (b) ideal selectivities (-□-, CO_2/N_2; -Δ-, CO_2/CH_4) of neat Pebax1657 membrane and NOHM-I-HPE/Pebax1657 MMMs at 1 bar and 23 °C.

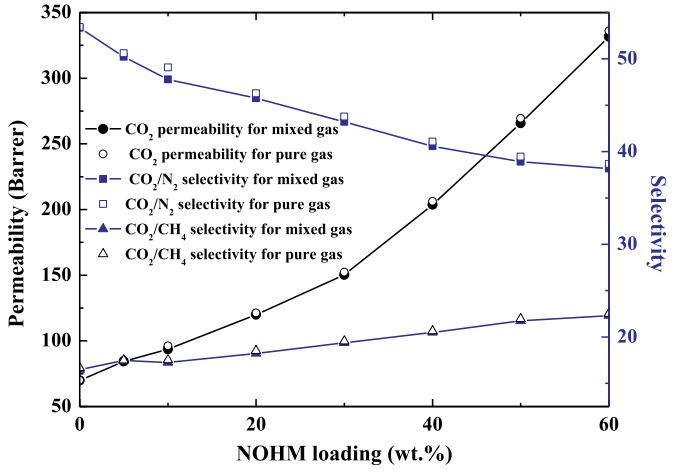

Fig. 9. Effect of NOHM-I-HPE loading on permeabilities and selectivities of NOHM-I-HPE/Pebax1657 MMMs for mixed (closed symbols) and pure gases (open symbols) at 1 bar and 23 °C.

solubility and diffusion (as can be seen from Eq. (5)). As explained in the section of 4.5, the permeability of CO_2 for the NOHM-I-HPE/Pebax1657 MMMs was mainly influenced by solubility, whereas those of N_2 and CH_4 were dominated by diffusion. For all the three gases, an increase in NOHM-I-HPE loading resulted in the increase of both gas diffusion and solubility coefficient (as shown in Figs. 6(a) and 7(a)), thus promoting the enhanced permeability. This result indicated that the addition of NOHM-I-HPE into the Pebax1657 improved gas transport properties of the MMM.

The next question was what were the selectivities of CO_2/CH_4 and CO_2/N_2 separations and what was the effect of the NOHM-I-HPE loading on the separation efficiency. Fig. 8(b) show the effect of NOHM-I-HPE loading on ideal selectivities of MMMs for pure gases at 1 bar and 23 °C. Also, to testify the separation performance of NOHM-I-HPE/Pebax1657 MMMs for gas mixtures, the permeation data of mixed gases of CO_2/CH_4 (30/70 vol.%) and CO_2/N_2 (15/85 vol.%) for membranes containing different NOHM-I-HPE content were measured at 23 °C and 1 bar. Fig. 9 shows the effect of NOHM-I-HPE loading on permeabilities and selectivities of MMMs for pure gases and mixed gases at 1 bar and 23 °C. It was obvious that the separation performances of MMMs for gas mixtures were good agreement with the data for pure gases.

As shown in Figs. 8(b) and 9, with an increase in NOHM-I-HPE

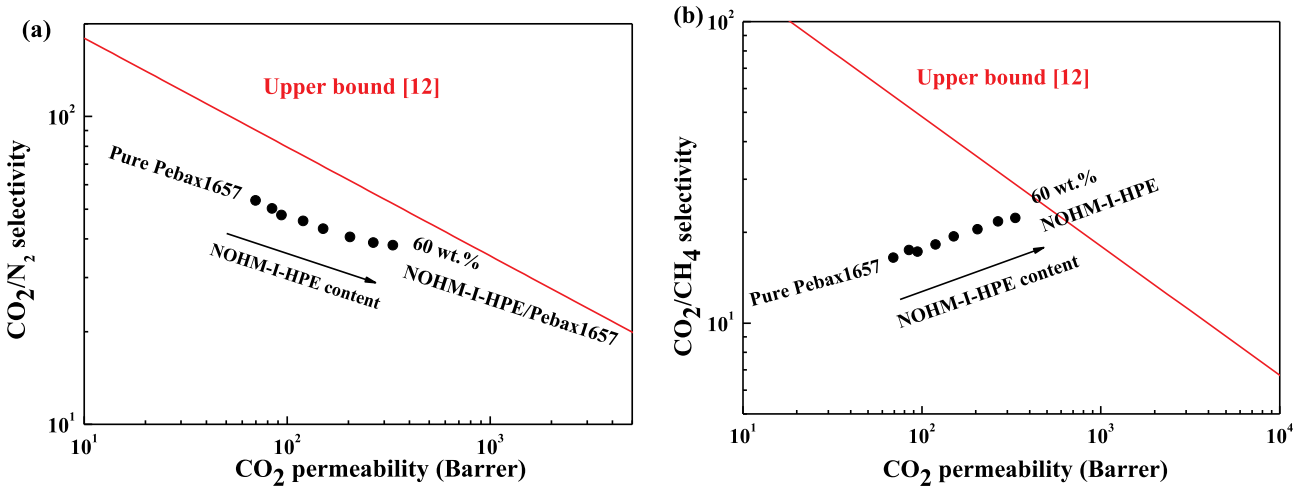

Fig. 10. Separation performances of NOHM-I-HPE/Pebax1657 MMMs with different NOHM-I-HPE loadings in terms of (a) CO_2/N_2 selectivity and (b) CO_2/CH_4 selectivity vs. CO_2 permeability and their comparisons to Robeson's upper bound.

loading, CO_2/N_2 selectivity of the NOHM-I-HPE/Pebax1657 MMMs showed a gradual decreasing trend, which was caused by a fact that the increase of CO_2 solubility was overcome by the higher diffusion of N_2 at higher NOHM-I-HPE loading (Figs. 6 and 7). However, with the increasing NOHM-I-HPE content from 0 wt% to 60 wt%, the selectivity of CO_2 to CH_4 for mixed gases increased from 16.50 to 22.31 (as shown in Fig. 9). The similar result has been reported by Wang et al. [36] that CO_2/CH_4 selectivity of the PEG20000/Pebax1657 membrane increased with the incorporation of high molecular PEG-based weight polymer, such as PEG20000. However, incorporating low molecular PEG-based polymers, such as PEG200, PEG400 and PEG600, led to a decrease of CO_2/CH_4 selectivity [6,22,36]. Reijerkerk et al. reported that with the increasing PEG200 content to 50 wt%, CO_2/CH_4 selectivity of the Pebax1657/PEG200 blended membrane decreased to 15.7 at a temperature of 35 °C and a feed pressure of 4 bar [6]. The results obtained in this work further testified that the membranes containing Pebax1657 and polymer with high EO content would be more effective for the separation of CO_2/CH_4 streams.

But since it is known that the selectivity decreases with the permeability, it was important to evaluate these findings against the well-known Robeson's upper bound [12] developed for polymeric membranes. As expected from the permability and selectivity results discussed earlier, the mixed matrix membranes containing NOHM-I-HPE significnatly improved both CO_2 permeability and CO_2/CH_4 selectivity and the slope of their relationship as a function of the NOHM-I-HPE loading was clearly positive towards the Robeson's upper bound (Fig. 10(b)). In other words, with higher NOHM-I-HPE loadings better separation between CO_2 and CH_4 was achived. The effect of the NOHM-I-HPE loading on the CO_2 and N_2 separation was less significant. However, as shown in Fig. 10(a) the rate of decrease in selectivity as a function of CO_2 permability was smaller than that of the Robenson's upper bound. This behavior suggested that the addition of NOHM-I-HPE improved the CO_2 permeability of the mixed matrix membrane while maintaining the selectivity CO_2 to N_2.

It is worth mentioning that the feed pressure tested in this work was only 1 bar. The NOHM-I-HPE/Pebax1657 MMMs might have surpassed the limit of the Robeson's upper bound (2008) if higher feed pressures were used (unfortunately the maximum pressure of our testing unit is 1 bar), because CO_2 capability of NOHM-I-HPE increases with the increasing CO_2 partial pressure [27]. Also, the existence of strong intermolecular interactions between water molecules and the poly(ethylene glycol) component of NOHMs, causing the drastic decrease in the NOHMs' viscosity with the addition of water [37]. Therefore, an optimal water content leading to the best trade-off for the given CO_2 capture conditions. In the following work, on the basis of MMMs, the composite membranes will be prepared, as well as the effect of different parameters (especially the water content) on separation performances of mixed gases for the composite membranes will be investigated in our following work in detail.

5. Conclusion

The NOHM-I-HPE/Pebax1657 MMMs with different NOHM-I-HPE loadings are successfully prepared by incorporating NOHM-I-HPE into Pebax1657 polymer. Characterization results indicate that the addition of NOHM-I-HPE resultes in structural and morphological changes of the Pebax1657-based membrane, and a higher NOHM-I-HPE loading resultes in a higher EO content and lower crystallinity in the NOHM-I-HPE/Pebax1657 MMMs. Consequently, diffusion coefficients for CO_2, N_2 and CH_4 show significant increases with a higher NOHM-I-HPE loading. As NOHM-I-HPE loading increases to 60 wt%, solubility coefficient of CO_2 is greatly increased from 1.16 to 3.84 cm^3 (STP)/(cm^3·bar) due to higher EO content in the mixed matrix membranes. This study shows that the newly developed NOHM-I-HPE/Pebax1657 membranes can improve both gas permeability and CO_2/CH_4 selectivities compared to the neat Pebax1657. CO_2 permeability of the NOHM-I-HPE/Pebax1657 MMM with 60 wt% NOHM-I-HPE loading is 335.93 Barrer, which is almost five times than that of the neat Pebax1657 membrane. Although the selectivity of CO_2 to N_2 shows a slight decrease, CO_2/CH_4 selectivity is enhanced from 16.50 to 22.31. All of these findings indicate that the NOHM-I-HPE/Pebax1657 MMMs are very promising candidates for CO_2 separation and its performance may further be improved by incorporating the functional groups in NOHMs that are more basic than EO groups.

Author contributions

Junfeng Wang designed the experiments and wrote the paper. Ming Gao synthesized NOHM-I-HPE. Wenjuan Fang executed the experiments. Jianquan Luo guided the experiments and revised the paper. Yinhua Wan, Ah-Hyung Alissa Park, Suojiang Zhang and Xiangping Zhang supervised the project and revised the paper.

Acknowledgements

This work was supported by the Fujian Institute of Innovation, Chinese Academy of Sciences (FJCXY18040101), the National High Technology Research and Development Program of China (863 Program, Grant no. 2014AA021006) and United States National Science Foundation (CBET 1231393).

Appendix A. Supplementary data

Supplementary data to this article can be found online at https://doi.org/10.1016/j.memsci.2019.04.079.

References

[1] M.K. Mondal, H.K. Balsora, P. Varshney, Progress and trends in CO_2 capture/separation technologies: a review, Energy 46 (2012) 431–441.
[2] Y. Park, D. Shin, Y.N. Jang, A.-H.A. Park, CO_2 Capture capacity and swelling measurements of liquid-like nanoparticle organic hybrid materials via Attenuated Total Reflectance Fourier Transform Infrared spectroscopy, J. Chem. Eng. Data 57 (2012) 40–45.
[3] J.L. Anthony, J.L. Anderson, E.J. Maginn, J.F. Brennecke, Anion effects on gas solubility in ionic liquids, J. Phys. Chem. B 109 (2005) 6366–6374.
[4] U. Desideri, R. Corbelli, CO_2 capture in small size cogeneration plants: technical and economical considerations, Energy Convers. Manag. 39 (1998) 857–867.
[5] A. Meisen, S. XiaoShan, Research and development issues in CO_2 capture, Energy Convers. Manag. 38 (1997) 37–42.
[6] S.R. Reijerkerk, M.H. Knoef, K. Nijmeijer, M. Wessling, Poly(ethylene glycol) and poly(dimethyl siloxane): combining their advantages into efficient CO_2 gas separation membranes, J. Membr. Sci. 352 (2010) 126–135.
[7] J.F. Wang, J.Q. Luo, S.C. Feng, H.R. Li, Y.H. Wan, X.P. Zhang, Recent development of ionic liquid membranes, Green Energy Environ. 1 (2016) 43–61.
[8] G. Qi, Y. Wang, L. Estevez, X. Duan, N. Anako, A.-H.A. Park, W. Li, C.W. Jones, E.P. Giannelis, High efficiency nanocomposite sorbents for CO_2 capture based on amine-functionalized mesoporous capsules, Energy Environ. Sci. 4 (2011) 444–452.
[9] J.C. Hicks, J.H. Drese, D.J. Fauth, M.L. Gray, G. Qi, C.W. Jones, Designing adsorbents for CO_2 capture from flue gas-hyperbranched aminosilicas capable of capturing CO_2 reversibly, J. Am. Chem. Soc. 130 (2008) 2902–2903.
[10] K. Ghosal, B.D. Freeman, Gas separation using polymer membranes: an overview, Polym. Adv. Technol. 5 (1994) 673–697.
[11] C.E. Powell, G.G. Qiao, Polymeric CO_2/N_2 gas separation membranes for the capture of carbon dioxide from power plant flue gases, J. Membr. Sci. 279 (2006) 1–49.
[12] L.M. Robeson, The upper bound revisited, J. Membr. Sci. 320 (2008) 390–400.
[13] L.A. Utracki, History of commercial polymer alloys and blends, Polym. Eng. Sci. 35 (1995) 2–17.
[14] Y.Y. Wang, H.Y. Li, G.X. Dong, C. Scholes, V. Chen, Effects of fabrication and operation conditions on CO_2 separation performance of PEO-PA block copolymer membranes, Ind. Eng. Chem. Res. 54 (2015) 7273–7283.
[15] H.Z. Chen, Y.C. Xiao, T.-S. Chung, Synthesis and characterization of poly(ethylene oxide) containing copolyimides for hydrogen purification, Polymer 51 (2010) 4077–4086.
[16] M.M. Rahman, V. Filiz, S. Shishatskiy, C. Abetz, P. Georgopanos, M.M. Khan, S. Neumann, V. Abetz, Influence of poly(ethylene glycol) segment length on CO_2 permeation and stability of Polyactive membranes and their nanocomposites with PEG POSS, Appl. Mater. Interfaces 7 (2015) 12289–12298.
[17] J.H. Kim, S.Y. Ha, Y.M. Lee, Gas permeation of poly(amide-6-*b*-ethylene oxide) copolymer, J. Membr. Sci. 190 (2001) 179–193.
[18] H.B. Park, S.Y. Ha, Y.M. Lee, Percolation behavior of gas permeability in rigid-flexible block copolymer membranes, J. Membr. Sci. 177 (2000) 143–152.
[19] M.E. Rezac, T. John, Correlation of penetrant transport with polymer free volume: additional evidence from block copolymers, Polymer 39 (1998) 599–603.
[20] H. Chen, Y. Xiao, T.-S. Chung, Synthesis and characterization of poly(ethylene oxide) containing copolyimides for hydrogen purification, Polymer 51 (2010) 4077–4086.
[21] V.I. Bondar, B.D. Freeman, I. Pinnau, Gas transport properties of poly(ether-*b*-amide) segment block copolymers, J. Polym. Sci., Part B: Polym. Phys. 38 (2000) 2051–2062.
[22] A. Car, C. Stropnik, W. Yave, K.-V. Peinemann, PEG modified poly(amide-*b*-ethylene oxide) membranes for CO_2 separation, J. Membr. Sci. 307 (2008) 88–95.
[23] S.R. Reijerkerk, M. Wessling, K. Nijmeijer, Pushing the limits of block copolymer membranes for CO_2 separation, J. Membr. Sci. 378 (2011) 479–484.
[24] S.R. Reijerkerk, M.H. Knoef, K. Nijmeijer, M. Wessling, Poly(ethylene glycol) and poly(dimethyl siloxane): combining their advantages into efficient CO_2 gas separation membranes, J. Membr. Sci. 352 (2010) 126–135.
[25] A. Ghadimi, M. Amirilargani, T. Mohammadi, N. Kasiri, B. Sadatnia, Preparation of alloyed poly(ether block amide)/poly(ethylene glycol diacrylate) membranes for separation of CO_2/H_2 (syngas application), J. Membr. Sci. 458 (2014) 14–26.
[26] W. Yave, A. Car, K.V. Peinemann, Nanostructured membrane material designed for carbon dioxide separation, J. Membr. Sci. 350 (2010) 124–129.
[27] K.-Y.A. Lin, A.-H.A. Park, Effects of bonding types and functional groups on CO_2 capture using novel multiphase systems of liquid-like nanoparticle organic hybrid materials, Environ. Sci. Technol. 45 (2011) 6633–6639.
[28] C. Petit, Y. Park, K.-Y.A. Lin, A.-H.A. Park, Spectroscopic investigation of the canopy configurations in nanoparticle organic hybrid materials of various grafting densities during CO_2 capture, J. Phys. Chem. C 116 (2012) 516–525.
[29] Y. Park, J. Decatur, K.-Y.A. Lin, A.-H.A. Park, Investigation of CO_2 capture mechanisms of liquid-like nanoparticle organic hybrid materials via structural characterization, Phys. Chem. Chem. Phys. 13 (2011) 18115–18122.
[30] K.-Y.A. Lin, C. Petit, A.-H.A. Park, Effect of SO_2 on CO_2 capture using liquid-like nanoparticle organic hybrid materials, Energy Fuels 27 (2013) 4167–4174.
[31] J.M. Prausnitz, R.N. Lichtenthaler, E.D. de Azevedo, Molecular Thermodynamics of Fluid-phase Equilibria, third ed., Prentice-Hall, Upper Saddle River, NJ, 1999, p. 144.
[32] Q. Gan, D. Rooney, M. Xue, G. Thompson, Y. Zou, An experimental study of gas transport and separation properties of ionic liquids supported on nanofiltration membranes, J. Membr. Sci. 280 (2006) 948–956.
[33] R.S. Murali, A.F. Ismail, M.A. Rahman, S. Sridhar, Mixed matrix membranes of Pebax-1657 loaded with 4A zeolite for gaseous separations, Separ. Purif. Technol. 129 (2014) 1–8.
[34] K. Ramasubramanian, Y.A. Zhao, W.S. Winston Ho, CO_2 capture and H_2 purification: prospects for CO_2-selective membrane processes, AIChE J. 59 (2013) 1033–1045.
[35] P. Bernardo, J.C. Jansen, F. Bazzarelli, F. Tasselli, A. Fuoco, K. Friess, P. Izák, V. Jarmarová, M. Kačírková, G. Clarizia, Gas transport properties of Pebax R/room temperature ionic liquid gel membranes, Separ. Purif. Technol. 97 (2012) 73–82.
[36] S. Wang, Y. Liu, S. Huang, H. Wu, Y. Li, Z. Tian, Z. Jiang, Pebax–PEG–MWCNT hybrid membranes with enhanced CO_2 capture properties, J. Membr. Sci. 460 (2014) 62–70.
[37] C. Petit, S. Bhatnagar, A.-H.A. Park, Effect of water on the physical properties and carbon dioxide capture capacities of liquid-like Nanoparticle Organic Hybrid Materials and their corresponding polymers, J. Colloid Interface Sci. 407 (2013) 102–108.
[38] Y. Dai, X.H. Ruan, Z.J. Yan, K. Yang, M. Yu, H. Li, W. Zhao, G.H. He, Imidazole functionalized graphene oxide/PEBAXR mixed matrix membranes for efficient CO_2 capture, Separ. Purif. Technol. 166 (2016) 171–180.
[39] L. De Lorenzo, E. Tocci, A. Gugliuzza, E. Drioli, Assembly of nanocomposite PEBAX membranes: a complementary study of affinity and clusterization phenomena, J. Membr. Sci. 421–422 (2012) 75–84.
[40] V. Bondar, B.D. Freeman, I. Pinnau, Gas sorption, characterization of poly(ether-*b*-amide) segmented block copolymer, J. Polym. Sci., Part B: Polym. Phys. 37 (1999) 2463–2475.
[41] H. Rabiee, A. Ghadimi, S. Abbasi, T. Mohammadi, CO_2 separation performance of poly(ether-*b*-amide6)/PTMEG blended membranes: permeation and sorption properties, Chem. Eng. Res. Des. 98 (2015) 96–106.
[42] M.M. Rahman, V. Filiz, S. Shishatskiy, C. Abetz, S. Neumann, S. Bolmer, M.M. Khan, V. Abetz, PEBAXR with PEG functionalized POSS as nanocomposite membranes for CO_2 separation, J. Membr. Sci. 437 (2013) 286–297.
[43] Y. Li, T.-S. Chung, Molecular-level mixed matrix membranes comprising Pebax R and POSS for hydrogen purification via preferential CO_2 removal, Int. J. Hydrogen Energy 35 (2010) 10560–10568.
[44] R. Silverstein, F. Webster, D. Kiemle, Spectrometric Identification of Organic Compounds, John Wiley & Sons, 2015.
[45] Q. Gan, D. Rooney, M. Xue, G. Thompson, Y. Zou, An experimental study of gas transport and separation properties of ionic liquids supported on nanofiltration membranes, J. Membr. Sci. 280 (2006) 948–956.